Spin dependent electrochemistry: Focus on chiral vs achiral charge transmission through 2D SAMs adsorbed on gold

Spin dependent electrochemistry: focus on chiral vs achiral charge transmission through 2D SAMs adsorbed on gold.

Massimo Innocenti[a], Maurizio Passaponti[a], Walter Giurlani[a], Agnese Giacomino[b],

Luca Pasquali[cde], Roberto Giovanardi[e], Claudio Fontanesi[e]*.

[a]*Dept. of Chemistry, University of Firenze, via della Lastruccia 3, 50019 Sesto Fiorentino, Firenze, Italy.*

[b]*Dept. of Drug Science and Technology, University of Torino, Via Giuria 9, 10125 Torino, Italy*

[c]*IOM-CNR Institute, Area Science Park, SS 14 Km, 163.5, Basovizza, 34149 Trieste, Italy*

[d]*Dept. of Physics, University of Johannesburg, P.O. Box 524, Auckland Park 2006, South Africa*

[e]*DIEF, University of Modena and Reggio Emilia, via Vivarelli 10, 41125 Modena, Italy.*

Abstract

The efficiency of charge transmission in chiral compared to achiral molecular systems, of structurally related compounds, is probed via cyclic voltammetry measurements. For such a purpose five different thiols have been selected two achiral (i.e. 3-mercaptopropionic acid (MPA) and 8-mercapto-1-octanol (M8O)) and three chiral (i.e. L- and D-cysteine (Lcys, Dcys) and D-penicillamine (Dpen)). These compounds are used to form 2D self-assembled monolayers (SAM)on gold. Cyclic voltammetry (CV) measurements, by using the potassium hexacyanoferrate(II)/potassium hexacyanoferrate(III) (Fe3Fe2) redox couple, are exploited to probe the charge transfer ability of the electrode|SAM|solution interface. In particular, MPA, Lcys and Dpen compounds are selected due to their quite similar structural and geometrical characteristics (virtually the same molecular length and terminal groups). M8O is a longer SAM forming thiol, which was selected as a reference blocking electrode compound. The comparison of the cyclic voltammetry data shows that a better ability in the charge transmission is obtained when chiral SAM are used; namely in the case of L-cysteine and D-penicillamine. This result can be related to the spin filtering ability of chiral compounds: chiral induced spin selectivity (CISS) effect. As rationalized on the basis of theoretical values of optical rotation (OR), calculated at the CAMB3LYP/6-31G(d,p) level of the theory.

Keywords: spin dependent electrochemistry, cysteine, penicillamine, cyclic voltammetry, DFT

This paper is respectfully dedicated to Prof. Claudine Buess-Herman in view of her outstanding achievements, in the study of 2D phase transition of monolayers adsorbed at the electrode solution|interface.

Correspondence should be addressed to: claudio.fontanesi@unimore.it

1. Introduction

The study of the 2D liquid-like → solid-like phase transition occurring in monolayers of organic compounds adsorbed at the mercury|aqueous-solution interface, is a quite exciting and challenging area of scientific research. On this specific subject, which finds its natural place within the chapter of interfacial physical chemistry, a number of seminal papers are due to Claudine Buess-Herman [1–4], together with important articles authored by Robert De Levie [5,6], Wandlowski and Retter [7,8]. These works essentially relate to the point of view of pure scientific research, where the objective is the understanding of the physics underlying the formation of ordered, solid-like, films of low dimensionality[2,4,5]. Also, with reference to the 2D liquid-like to solid-like phase transition kinetics. Such studies revealed to foster and nourish fundamental research in the field of low dimensional systems [9,10]. Within this picture, the study of 2D ordered adsorbed monolayers on the mercury electrode offered, and offers, a number of experimental advantages i) the mercury surface is almost perfectly smooth, being a liquid ii) allowing to control the formation of the 2D solid like phase by switching (or even by scanning) the electrode potential to a suitable value at which the condensed phase is formed. This proves particularly useful in studies concerning the kinetics of formation of the ordered phase [2]. What is more, the kinetics can be monitored both in direct current experiments (potential steps, chronoamperometry), as well as in alternate current mode(i.e. measuring the impedance versus time curves at a fixed a.c. frequency).In general, these measurements are carried out applying a potential step and measuring the current (or the capacity) as a function of time[2,4,8,11–14]. Beyond the scientific interest it must be noted that a large class of organic compounds, showing the formation of a 2D solid-like phase on the Hg electrode, are purine basis. That is: molecules involved in the formation of supramolecular structures in both DNA and RNA macromolecules[15], thus these studies serve also helping to single out intermolecular interactions (pi-pi stacking, hydrogen-bond interactions) concerning the mimicking of much more complex self-organized biological systems. In particular, a fundamental contribution in the study of kinetic properties relevant to the nucleation and growth mechanism of 2D solid like films is due to Claudine Buess-Herman in a series of seminal papers on such an intriguing topic[1–3]. Notably also addressing the thermodynamic properties of the solid-like 2D ordered phase has been the subject of a number of papers aiming to rationalize the reole played by the molecular electronic structure in ruling the occurring of such a peculiar 2D phase transition[5,13,14].A re-

lated field of research concerns the much more ample area of studies devoted to prepare and characterize the 2D ordered ultra-thin films of thiols adsorbed on gold, with the formation of so-called self-assembled monolayers (SAM)[16–25]. Within the different thiol compounds a number of interesting fundamental studies relate to cysteine SAMs on gold, where systematic chemical and physical properties are studied and used for modellistic purposes, due to the simple structure of cysteine and the fact that good quality SAMs can be easily prepared [26–28]. Notably, also the formation of SAM obtained by exploiting the amino group adsorption capability has been observed on gold, and SAM of thiols on metals different from the gold, are investigated: glassy carbon, valve metals (Ni, Al, Cu) [29–32].Eventually, within this area of research also chemisorbed SAMs are currently investigated, i.e.2D ordered SAMs of organic compounds covalently bound to the surface (for instance glassy carbon [33] and silicon [34–37]).It must be noted that research concerning 2D SAM functionalized surface is also of importance in practical applications allowing for the production of hybrid interfaces used as sensors in analytical detection systems [38–40], organic-electronics [41–43] and optronics [44,45]. Remarkably, the charge transmission properties of 2D self-assembled monolayers are strictly relatedto the research activity concerning the field of organic electronics. Moreover, the "conductivity" through organic SAMs is correlated with the conductivity observed in organic systems upon chemical doping: the important field of conductive polymers [24,46]. Typically in electrochemistry, the charge transmission ability of hybrid metal/SAM electrodes is probed recording CVs of a suitable redox probe (quite often Fe3Fe2 [46–48]). Within this picture, a peculiar electrochemical behaviour is shown by chiral poly-alanine peptide SAMs adsorbed on gold. Where, despite the thickness of the monolayer, about 3.5 nm, and the expected non-conductive nature of a long saturated carbon chain, a quite efficient charge transfer efficiency has been detected when employing ferrocene as the redox couple [49,50], or related suitable organic compounds [51,52]. A similar high efficiency in charge transmission through long polyalanine systems has been exploited, and thus confirmed, in spin-dependent electrochemical (SDE) studies [53–57].

Thus, the aim of this paper is to show, and confirm, that there is a clear-cut efficiency difference in charge transmission between chiral and achiral SAMs (this is proved elaborating cyclic voltammetry measurements for a series of structurally related compounds able to form SAMs on gold). Moreover, this approach is pushed further, and a rationale is proposed underlying such a peculiar behaviour observed in chiral SAMs.

2. Chiral-induced spin selectivity (CISS) and spin-dependent electrochemistry

The chiral-induced spin selectivity (CISS) effect is based on the observation that the transmission of electrons through chiral molecular systems is spin specific, as first reported by Prof. Ron Naaman in 1999 [58]. In fact, it was proved that an Au surface coated with chiral SAMs ejects spin polarized photo-electrons, both using circular polarized, as well as unpolarized, photons. The development of the spin-dependent electrochemistry (SDE) concept follows the idea to study the CISS effect in electrochemistry, using working electrodes(WE) functionalized with chiral compounds [53]. In practice, spin injection can be obtained by using ferromagnetic materials in the presence of a magnetic field. A typical experimental setup in SDE experiment employs a ferromagnetic metal for the working electrode[1], which is kept in tight contact with a permanent magnet (on the side opposite to the solution). Then, spin polarization currents are measured as a function of the magnet orientation, the orientation of the magnet controls the spin-polarized (up or down) injection, thus allowing to measure the current (spin-polarized current) as a function of the spin (up or down) injection (i.e. as a function of the magnet orientation placed in tight contact with the WE) [59,56]. Note that, a definitive, and widely accepted, theoretical model able to explain in full why charge transmission in chiral systems is more effective is not yet available. Just to a lower level of complication, even a theory able to rationalize the electron conduction in organic systems (without the complication of symmetry specific constraints) is still open to study. The Landauerer model is within this context the most widespread accepted approach [60], but a definitive well-defined picture is still missing: topological, statistical based, quantum mechanical models are available in the literature [61,62]. Within this field the study of the mechanism of electron conduction in the specific case of Self-Assembled alkanethiol monolayer has also been tackled, by using the Simmons equation, and more in general leading to relationships in the form $J \propto e^{-\beta d}$ where d is the molecular length and β is found a parameter which depends on the applied bias [63,64]. Quite recently the influence of the presence of a model helical potential (due to the handedness of a chiral molecule) on the polarization of transmitted electrons has been theoretically proved [65–67].

[1]typically nickel

3. Experimental

3.1 Chemicals

All the compounds are reagent grade, and purchased from Sigma: 8-mercapto-1-octanol (M8O) 706922 CAS Number 33065-54-2,3-mercaptopropionic acid (MPA)M5801 CAS Number 107-96-0, L-cysteine (Lcys) 30089 CAS Number 52-90-4, D-penicillamine (Dpen) P4875, Potassium hexacyanoferrate(II) 455989 CAS Number 14459-95-1, potassium hexacyanoferrate(III) CAS Number 13746-66-2, KCl P9333 CAS Number: 7447-40-7. Quasi-Au(111) surfaces served as the working electrode: 200 nm gold thickness, on 5 nm Cr adhesion layer, on top of a silicon 0.5 mm thickness wafer, Si(100) Siltronix [68]. Before each measurement, the gold working electrode was polished with alumina paste (1 μm particles), sonicated in isopropanol solution for 10 min, and then subjected to "gentle" flame annealing: sixty seconds on an ethanol flame. Reagent grade water was obtained using a Milli-Q, Millipore, system.

3.2 Electrochemical Measurements.

Electrochemical measurements were carried out in a three-electrode cell using a large area Platinum wire as the counter electrode, and a silver wire as pseudo-reference electrode.Application of a suitable calibration procedure allowed to calibrating the measured potentials with respect to the saturated calomel electrode (SCE). A polycrystalline gold disk, quasi-Au(111), 10 mm in diameter served as the working electrode.All the electrochemical measurements were carried out by using an Autolab PGSTAT204 (Metrohm Autolab) potentiostat equipped with a frequency response analyser FRA32M module. Cyclic voltammetry (CV) were recorded as a function of the potential scan rate: 10, 25, 50, 100 250, 500 mV/s in a solution 1 mM potassium ferrocyanide, (Fe2) 1mM potassium ferricyanide (Fe3), 0.5 KCl water solution is the supporting electrolyte. Electrochemical impedance spectroscopy (EIS) measurements were performed in the range $10^5 - 0.1$ Hz with 10mV peak-to-peak potential amplitude, at a constant equilibrium potential: selected by measuring the relevant open-circuit potential (OCP) for each analysed solution. All of the solutions were prepared with ultrapure water (Milli-Q system from Millipore). An incubation time of 12 hours was used to produce SAM functionalized gold surfaces. The concentration of the incubation solution was 10 mM. This at variance for Lcys (and Dcys) for both these compounds it was used a saturated solution.

3.3 Atomic force microscopy (AFM) measurements.

Atomic force microscopy (AFM) (PicoSPM, Molecular Imaging, Tempe, AZ, USA) was used to acquire images of the SAM functionalized surfaces (512 px x 512 px, 5µm x 5µm) and evaluate the roughness. The measurements were performed in contact mode with a non-conductive Si_3N_4 triangular cantilever (NP-S10, Veeco, Plainview, NY, USA): 0.4 - 0.7 µm range in depth, 0.12 N/mforce constant, 0.5 V force set point and 1.21 l/s speed.

3.4 Theoretical calculations.

Theoretical calculations have been performed at CAM-B3LYP/cc-pVTZ level of the theory using Gaussian [69]. Full geometry optimization, without any symmetry constraint, was followed by density functional (DFT) time dependent (TD) calculations of the absorption electronic spectrum, with also the calculation of the optical rotation property response (circular dichroism, CD) and optical rotation (OR). The optical rotation (OR) was calculated at an exciting energy wavelength of 589.3 nm, i.e. the energy of typical sodium lamp light source.

3.5 X-ray photo-electron (XPS) measurements

X-ray photo electron spectroscopy measurements were carried out at normal emission, with a VG XR3 double anode, and a X ray source delivering Mg Ka photons at 15 kV and 15mA.A CLAM2 VG hemispherical analyser driven at constant pass energy was employed. Survey spectra were recorde with an analyser resolution of 2 eV. Elemental spectra feature a higher resolution of 0.5 eV. Results are reported in the Supporting Information.

4. Results and Discussion

Chart 1 sets out the molecular structures of the thiols used for the gold surfaces functionalization. These compounds have been selected on the basis of some precise criteria: **M8O** isa rather long alkyl chain molecule able to form a, quasi-blocking, non-conducting SAM **MPA** is an achiral molecule featuring a short alkyl chain carbon backbone, **Lcys** and **Dpen** are chiral compounds and epitome molecules used in previous spin-dependent electrochemistry studies [29,70,71]. MPA, Lcys and Dpen feature the same alkyl carbon backbone structure, which means that they form SAMs of the same thickness (compare Chart 1). Remarkably also the functional groups are exactly the same, with the carboxylic group facing the solution.

Chart 1.

Achiral

M8O

$HSCH_2(CH_2)_6CH_2OH$

MPA

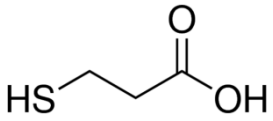

Chiral

L-cysteine (Lcys)

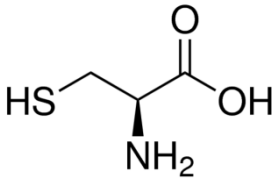

D-penicillamine (Dpen)

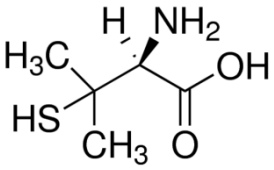

4.1 Cyclic voltammetry

Figure 1a shows typical CV curves recorded using a quasi-Au(111) functionalized working electrode, at a fixed value of scan rate, ν,of 50 $mV\ s^{-1}$. Qualitatively, quite similar CVs are obtained in the 20 to 500 mV s-1 potential scan rate.The same reciprocal ordering in the CV curves is maintained, i.e. when the CV curves of the different compounds are compared at a given value of potential scan rate, the reversibility hierarchy results bare Au ≅ Au|Lcys > Au|Dpen > Au|MPA > Au|M8O (for the sake of comparison, Figure 1SI shows CV curves for a gold D-cysteine functionalized electrode, as a function of the potential scan rate).The CV curve of a Fe3Fe2 redox couple on the bare-Au surface, Figure 1 black curve, shows an almost ideal pattern with a 78 mV anodic vs cathodic peak-to-peak potential separation (ΔE_p),$\Delta E_p = E_{peak\ anodic} - E_{peak\ cathodic}$, moreover the ratio between the anodic and cathode peak currents is quite close to unity. These results serve as a cross check to confirm the high quality of our pristine gold surface. The CV observed with the Lcys functionalized gold surface is virtually coincident with that of the bare gold surface. Also the application of any possible fitting procedure is useless in differentiating the bare and Lcys CVs, due to the negligible difference observed between these two curves: compare the black (bare-Au) and red (Lcys) curves in Figure 1a.What is more, also the pattern $\Delta E_p\ vs\ \nu$ of the Au|Lcys functionalized electrode is almost coincident with that of the bare-Au electrode, compare black

and red curves in Figure 1b, which are the bare and A|Lcys electrodes, respectively. The results obtained using the chiral D-penicillamine are similar to those obtained with L-cysteine (the structures of Lcys and Dpen differ just for the presence of two side chain methyl groups), but a not negligible deviation from the bare-reference bare gold surface is evident. In particular, the ΔE_pvalue, $0.130\ V$, is slightly, but significantly, larger than that of the bare Au and Au|Lcys systems. Indeed, the pattern $\Delta E_p\ vs\ \nu$ of the Au|Dpen functionalized electrode is definitively different with respect to those of the bare-Auand Au|Lcys electrodes: compare blue, red and black curves in Figure 1b, Au/Dpen,A clear-cut difference in the electrochemical behaviour is evident for the Au|MPA electrode, the relevant CV and $\Delta E_p\ vs\ \nu$ curves are shown in Figure 1a and 1b (green line), respectively. Still a quasi-reversible behaviour can be inferred from CV curves, that is a rather symmetrical CV curve around the OCP potential and the anodic to cathodic current ratio is close to unity. Nonetheless, the peak-to-peak potential difference is significantly larger,for MPA $\Delta E_p = 0.190\ V$ at$\nu = 50\ mV\ s^{-1}$, than that of the bare-Au surface and the OCP is shifted to more positive potentials. Also the pattern of the $\Delta E_p\ vs\ \nu$ graph shows a marked deviation, getting larger and larger, at increasing the potential scan rate, compare Figure 1b green curve.Eventually the Au|M8O electrode, it forms the longest and less conductive SAM, andindeed the overall electrochemical behaviour is characterized by lower current values and by a clear shift of the OCP to more positive potentials, also the peak-to-peak potential difference is the largest and features the largest gradient as a function of the scan rate, compare Figure 1b.As a further check, the relationship between the current of the anodic peak as a function of the square of the potential scan rate,ν^2, is found linear, as it is theoretically expectedin the case of a nernstian (fast and reversible), and diffusion controlled, charge transfer mechanism, the$I_p\ vs.\ \nu^2$pattern should be linear [72].

Figure 1

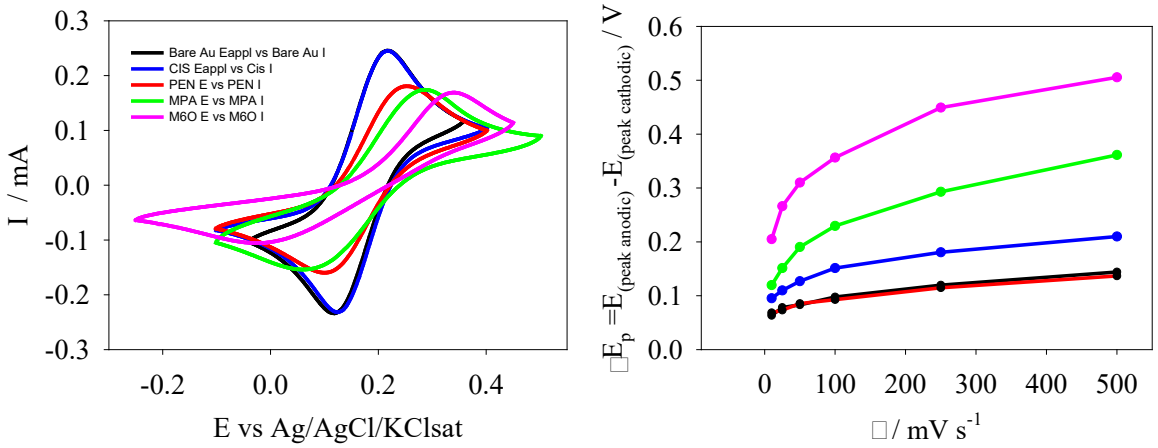

Figure 1. a) CV curves Fe3Fe2 5mM solution, 0.5 M KCl in water: black (bare Au), blue (Lcys), red (Dpen), green (MPA), magenta (M8O). b) Graph of ΔE_p $vs.v^2$ data obtained by elaborating the CV curves of Fe3Fe2 5mM 0.5 M KCl aqueous soltion: black (bare Au), blue (Lcys), red (Dpen), green (MPA), magenta (M8O).

4.2 Electrochemical impedance

Figure 2

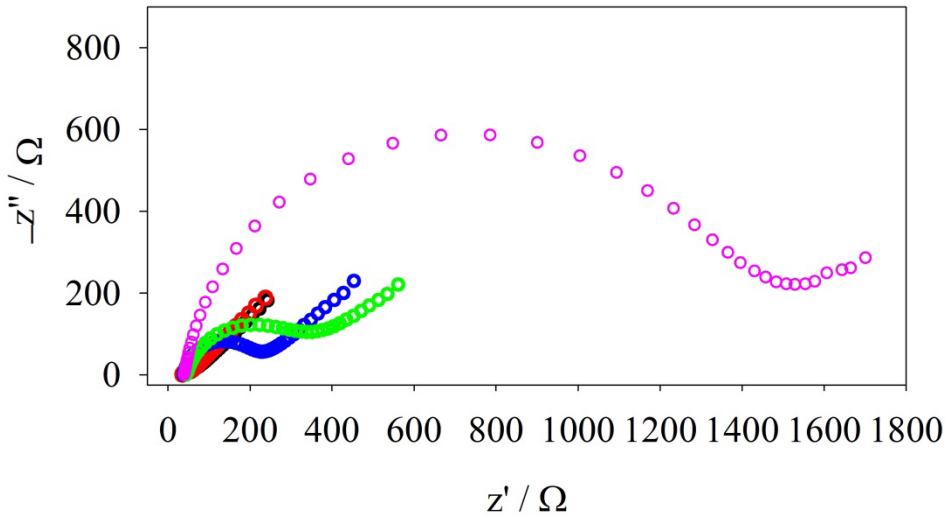

Figure 2. Electrochemical impedance spectra recorded in the 10^5 – 0.1 Hz range with a 10 mV peak-to-peak amplitude 10 sinusoidal perturbing signal. EIS curves are recorded at the equilibrium standard potential of a Fe3Fe2 5mM, 0.5 M KCl aqueous solution: black (bare Au), blue (Au|Lcys), red (Au|Dpen), green (Au|MPA), magenta (Au|M8O).

Figure 2 sets out EIS curves recorded at the equilibrium standard potential: Fe3Fe2 5mM, 0.5 M KCl aqueous solution. On the whole, the EIS experimental outcomeis fully consistent with the electrochemical pictureobtained by elaborating the CV curves. From a qualitative point of view, the same EIS pattern is obtainedfor all the five systems here investigated: a high-frequency semicircle, which is followedby aconstant phase angle pattern in the low frequency region(Warburg diffusion behaviour). The different spectra were fitted with a parallel capacitance (representative of the interfacial double layer, C_{dl}) and resistor, R_{ct} (representative of the charge transfer rate constant, K_{ct}) circuit in series with a Warburg type element. TheR_{ct}values are found to increase in the order (the relevant values of K_{ct} decrease) bare gold(30 Ω) < Lcys|Au (35 Ω)< Dpen|Au (260 Ω)< MPA|Au (410 Ω)< M8O|Au (1500 Ω). Impedance spectra were simulated by using the Autolab NOVA EIS spectrum analyser program[73].

4.3 Theoretical calculation of electronic spectra

Theoretical calculations of the electronic UV/Vis and relevant circular dichroism (CD) spectra of both Lcys and Dpen show a rather similar outcome, compare Figure 3.Time-dependent density

functional theory (TD-DFT) calculations were carried out considering the first 20 excited states. Note that,on the whole the CD spectrum of Lcys shows slightly larger R(strength) values. Indeed, the calculation of the optical rotation (OR) yields 217.7 deg. for Lcys; while a smaller value (the absolute value of the OR value must be considered) of–110.4 deg. is obtained for Dpen. Thus, if we assume that a larger OR value can be considered as a more prominent chirality manifestation[57],the ordering obtained on the basis of the OR values allows to rationalize the better ability of Lcys in the charge transmission process with respect to Dpen, as connected to a "more preeminent" chiral character of Lcys with respect to Dpen.

Figure3

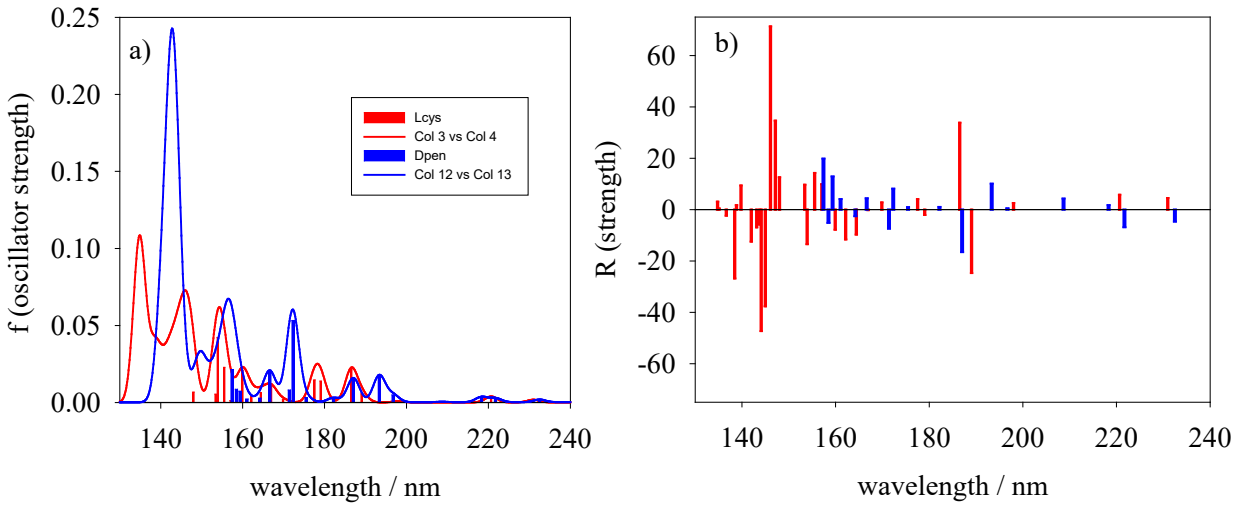

Figure 3. a) CAMB3LYP/6-31G(d,p) TD-DFT theoretical UV/Vis spectra calculated for Lcys (red) and Dpen (blue). b) the relevant R(Strength) circular dichroism spectra: Lcys (red bar) and Dpen (blue bar)

4.4 Atomic force microscopy

AFM images were recorded to assess the influence of the functionalization process on the morphology of the surface. Figure 4a shows the surface morphology of the bare quasi-Au(111) pristine surface. Figure 4b and 4c sets out, as an example, the surface morphology of the functionalized Au|Lcys and Au|Dpen surfaces. Qualitatively,the samples appear rather flat at the nanoscale, confirming that the functionalization and the sustained treatments did not end up in any dramatic damage of the surface.The root mean square (RMS) roughness, R_{rms}, values were also measured and used as an indication of the surface coarseness induced by functionalization using the different molecules here studied.

Figure 4

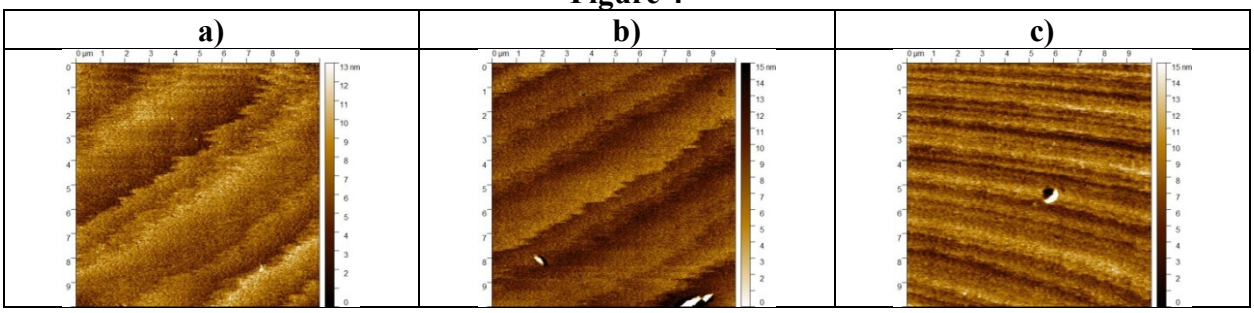

Figure 4. AFM scans of the electrodes, scan area 5.0 µm × 5.0 µm, surface morphology of a) bare gold b) Au|Lcys c) Au|Dpen.

The following R_{rms} values are obtained: bare quasi-Au(111) 1.59 (±0.2) nm, Au|Lcys 1.73 (±0.15) nm, Au|Dpen1.93 (±0.1) nm, Au|MPA 1.77 (±0.15) nm, Au|M8O 1.73 (±0.15) nm. As a whole, the variations of the R_{rms}values for the different samples are minimal and comparable with the roughness of the bare pristine quasi-Au(111) surface.Thus, we can conclude that the functionalization treatments do not result in a surface with higher roughness with respect to the original pristine gold, and that the different results observed in the electrochemical behaviour stem from the different structure of the compounds here studied rather than from geometrical inhomogeneity in the surfaces.

5. Conclusions

CV measurements using theFe3Fe2 redox couple are exploited to probe, in a systematic way, the charge transmission ability of chiral vs. achiral molecular systems,selectingfour structurally related organic compounds[46,51] (which means to probe the conductivity, i.e. the charge transmission *through* the SAM [61,74,75]). To this end, four structurally related organic compounds have been selected: two achiral and two chiral. This aiming to unravel quite recent and peculiarelectrochemical results obtained in the case of gold functionalized with chiral SAMs of large thickness:long polypeptide chains up to 3.5 nm(polyalanine featuring from 5 to 9 repeating units [15,49,50,54,55,76]) show an “anomalous” high charge transmission, a characteristic also exploited in so-called spin-dependent electrochemistry studies [56,77,78]. In general, the above mentioned picture is inferred on the observation of a quasi-reversible behaviour of Fe3Fe2 CV curves. Indeed in this work it is confirmed, in a systematic way, that chirality plays a fundamental role in the charge transmission. Please note that Lcys(the relevant CVs are virtually overlapping to those of the bare gold surface) is characterized by a larger optical activity with respect to Dpen. Thus if

we consider the OR as a measure of chirality manifestation, a hierarchy is here determined in terms of "chirality" and efficiency in the charge transmission process. To the best of our knowledge, this is the first report of such observation, which allows for a tight correlation between the "chiral character" of a chiral compound and the relevant ability in the charge-transmission property (which is also related to the CISS effect).

5. Acknowledgements

R.G. and C.F. gratefully acknowledge financial support for this research by the University of Modena and Reggio Emilia (Department of Engineering 'Enzo Ferrari': DIEF), through the "Spin-Dependent Electrochemistry", FAR2016 project. Prof. Ron Naaman, Weizmann Institute of Science, is gracefully acknowledged for helpful discussion and encouragement concerning development and application of the Spin-Dependent Electrochemistry concept.

References

[1] Cl. Buess-Herman, Non-faradaic phase transitions in adsorbed organic layers: Part I. General Theory, Journal of Electroanalytical Chemistry and Interfacial Electrochemistry. 186 (1985) 27–39. doi:10.1016/0368-1874(85)85752-X.

[2] Cl. Buess-Herman, Non-faradaic phase transitions in adsorbed organic layers: Part II. Experimental aspects, Journal of Electroanalytical Chemistry and Interfacial Electrochemistry. 186 (1985) 41–50. doi:10.1016/0368-1874(85)85753-1.

[3] C. Buess-Herman, C. Franck, L. Gierst, On the influence of molecular structure on the orientation and the occurrence of phase transitions in organic adsorbed layers at the mercury—water interface, Journal of Electroanalytical Chemistry. 329 (1992) 91–102. doi:10.1016/0022-0728(92)80210-U.

[4] M. Scharfe, Cl. Buess-Herman, Multiple metastable states in the two-dimensional condensation of uridine at the mercury electrode, Journal of Electroanalytical Chemistry. 366 (1994) 303–310. doi:10.1016/0022-0728(93)03040-V.

[5] R. De Levie, The dynamic double layer: Two-dimensional condensation at the mercury-water interface, Chem. Rev. 88 (1988) 599–609. doi:10.1021/cr00086a001.

[6] A. Popov, R. Naneva, N. Dimitrov, T. Vitanov, V. Bostanov, R. de Levie, Two-dimensional condensation of thymine on a basal face of a cadmium single crystal, Electrochimica Acta. 37 (1992) 2369–2371. doi:10.1016/0013-4686(92)85134-7.

[7] Th. Wandlowski, M. Heyrovsky, L. Novotny, Interfacial properties of uracil films adsorbed at the mercury/electrolyte interface, Electrochimica Acta. 37 (1992) 2663–2672. doi:10.1016/0013-4686(92)87067-A.

[8] U. Retter, Modelling of 2d first-order phase transitions in adsorption layers at the metal/electrolyte interface, Electrochimica Acta. 41 (1996) 2171–2174. doi:10.1016/0013-4686(96)00048-5.

[9] A.D. Yoffe, Electronic properties of low dimensional solids: The physics and chemistry of layer type transition metal dichalcogenides and their intercalate complexes, Solid State Ionics. 39 (1990) 1–7. doi:10.1016/0167-2738(90)90021-I.

[10] J.E. Moore, The birth of topological insulators, Nature. 464 (2010) 194–198. doi:10.1038/nature08916.

[11] L. Pospisil, Fractal character of compact layers of Tris(2,2'-bipyridine)cobalt(II) perchlorate formed at the mercury/solution interface by the electrochemical nucleation and growth mechanism, J. Phys. Chem. 92 (1988) 2501–2506. doi:10.1021/j100320a022.
[12] T. Wandlowski, E. Krestchmer, U. Retter, Investigation of the adsorption kinetics of 2,3-dimethylpyridine at the mercury/electrolyte interface, Journal of Electroanalytical Chemistry and Interfacial Electrochemistry. 224 (1987) 261–271. doi:10.1016/0022-0728(87)85097-0.
[13] C. Fontanesi, Entropy change in the two-dimensional phase transition of adenine adsorbed at the Hg electrode/aqueous solution interface, J. Chem. Soc., Faraday Trans. 90 (1994) 2925–2930. doi:10.1039/FT9949002925.
[14] C. Fontanesi, 2D Phase transition of organic molecules adsorbed at the Hg electrode/aqueous solution interface Part 2 Comparison of experimental data with model predictions, J. Chem. Soc., Faraday Trans. 94 (1998) 2417–2422. doi:10.1039/A803520B.
[15] S. Mishra, V.S. Poonia, C. Fontanesi, R. Naaman, A.M. Fleming, C.J. Burrows, The effect of oxidative damage on charge and spin transport in DNA, J. Am. Chem. Soc. (2018). doi:10.1021/jacs.8b12014.
[16] H.O. Finklea, Self-Assembled Monolayers on Electrodes, in: Encyclopedia of Analytical Chemistry, John Wiley & Sons, Ltd, 2006. http://onlinelibrary.wiley.com/doi/10.1002/9780470027318.a5315/abstract (accessed April 11, 2015).
[17] F. Loglio, M. Innocenti, F. D'Acapito, R. Felici, G. Pezzatini, E. Salvietti, M.L. Foresti, Cadmium selenide electrodeposited by ECALE: electrochemical characterization and preliminary results by EXAFS, Journal of Electroanalytical Chemistry. 575 (2005) 161–167. doi:10.1016/j.jelechem.2004.09.007.
[18] R. Guidelli, M.L. Foresti, M. Innocenti, Two-Dimensional Phase Transitions of Chemisorbed Uracil on Ag(111): Modeling of Short- and Long-Time Behavior, J. Phys. Chem. 100 (1996) 18491–18501. doi:10.1021/jp961663z.
[19] L. Wang, A. Lavacchi, M. Bevilacqua, M. Bellini, P. Fornasiero, J. Filippi, M. Innocenti, A. Marchionni, H.A. Miller, F. Vizza, Energy Efficiency of Alkaline Direct Ethanol Fuel Cells Employing Nanostructured Palladium Electrocatalysts, ChemCatChem. 7 (2015) 2214–2221. doi:10.1002/cctc.201500189.
[20] L. Becucci, M. Innocenti, E. Salvietti, A. Rindi, I. Pasquini, M. Vassalli, M.L. Foresti, R. Guidelli, Potassium ion transport by gramicidin and valinomycin across a Ag(111)-supported tethered bilayer lipid membrane, Electrochimica Acta. 53 (2008) 6372–6379. doi:10.1016/j.electacta.2008.04.043.
[21] M. Innocenti, F. Loglio, L. Pigani, R. Seeber, F. Terzi, R. Udisti, In situ atomic force microscopy in the study of electrogeneration of polybithiophene on Pt electrode, Electrochimica Acta. 50 (2005) 1497–1503. doi:10.1016/j.electacta.2004.10.034.
[22] M.L. Foresti, S. Milani, F. Loglio, M. Innocenti, G. Pezzatini, S. Cattarin, Ternary CdSxSe1-x Deposited on Ag(111) by ECALE: Synthesis and Characterization, Langmuir. 21 (2005) 6900–6907. doi:10.1021/la050176k.
[23] T. Doneux, C. Buess-Herman, M.G. Hosseini, R.J. Nichols, J. Lipkowski, Adsorption of 2-mercaptobenzimidazole on a Au(111) electrode, Electrochimica Acta. 50 (2005) 4275–4282. doi:10.1016/j.electacta.2005.01.063.
[24] Q. Rayée, N. Phuong Thu, T. Segato, M.-P. Delplancke-Ogletree, T. Doneux, C. Buess-Herman, Electrochemical synthesis of copper(I) dicyanamide thin films, Journal of Electroanalytical Chemistry. 819 (2018) 331–337. doi:10.1016/j.jelechem.2017.11.001.
[25] A. De Rache, I. Kejnovská, C. Buess-Herman, T. Doneux, Electrochemical and circular dichroism spectroscopic evidence of two types of interaction between [Ru(NH3)6]3+ and an elongated thrombin binding aptamer G-quadruplex, Electrochimica Acta. 179 (2015) 84–92. doi:10.1016/j.electacta.2015.05.023.

[26] G. Hager, A.G. Brolo, Adsorption/desorption behaviour of cysteine and cystine in neutral and basic media: electrochemical evidence for differing thiol and disulfide adsorption to a Au(111) single crystal electrode, Journal of Electroanalytical Chemistry. 550–551 (2003) 291–301. doi:10.1016/S0022-0728(03)00052-4.

[27] K. Arihara, T. Ariga, N. Takashima, K. Arihara, T. Okajima, F. Kitamura, K. Tokuda, T. Ohsaka, Multiple voltammetric waves for reductive desorption of cysteine and 4-mercaptobenzoic acid monolayers self-assembled on gold substrates, Physical Chemistry Chemical Physics. 5 (2003) 3758–3761. doi:10.1039/B305867K.

[28] S. Bengió, M. Fonticelli, G. Benítez, A.H. Creus, P. Carro, H. Ascolani, G. Zampieri, B. Blum, R.C. Salvarezza, Electrochemical Self-Assembly of Alkanethiolate Molecules on Ni(111) and Polycrystalline Ni Surfaces, The Journal of Physical Chemistry B. 109 (2005) 23450–23460. doi:10.1021/jp052915b.

[29] C. Fontanesi, F. Tassinari, F. Parenti, H. Cohen, P.C. Mondal, V. Kiran, A. Giglia, L. Pasquali, R. Naaman, New One-Step Thiol Functionalization Procedure for Ni by Self-Assembled Monolayers, Langmuir. 31 (2015) 3546–3552. doi:10.1021/acs.langmuir.5b00177.

[30] Z. Mekhalif, F. Laffineur, N. Couturier, J. Delhalle, Elaboration of Self-Assembled Monolayers of n-Alkanethiols on Nickel Polycrystalline Substrates: Time, Concentration, and Solvent Effects, Langmuir. 19 (2003) 637–645. doi:10.1021/la020332c.

[31] L. Tortech, Z. Mekhalif, J. Delhalle, F. Guittard, S. Géribaldi, Self-assembled monolayers of semifluorinated thiols on electrochemically modified polycrystalline nickel surfaces, Thin Solid Films. 491 (2005) 253–259. doi:10.1016/j.tsf.2005.06.090.

[32] S. Rajalingam, S. Devillers, J. Dehalle, Z. Mekhalif, A two step process to form organothiol self-assembled monolayers on nickel surfaces, Thin Solid Films. 522 (2012) 247–253. doi:10.1016/j.tsf.2012.08.036.

[33] P. Allongue, M. Delamar, B. Desbat, O. Fagebaume, R. Hitmi, J. Pinson, J.M. Saveant, Covalent modification of carbon surfaces by aryl radicals generated from the electrochemical reduction of diazonium salts, Journal of the American Chemical Society. 119 (1997) 201–207.

[34] C. Fontanesi, M. innocenti, D. Vanossi, E. Da Como, Ferrocene Molecular Architectures Grafted on Si(111): a theoretical calculation of the standard oxidation potentials and electron transfer rate constant., (n.d.).

[35] E.A. Dalchiele, A. Aurora, G. Bernardini, F. Cattaruzza, A. Flamini, P. Pallavicini, R. Zanoni, F. Decker, XPS and electrochemical studies of ferrocene derivatives anchored on n- and p-Si(1 0 0) by Si–O or Si–C bonds, Journal of Electroanalytical Chemistry. 579 (2005) 133–142. doi:10.1016/j.jelechem.2005.02.002.

[36] P. Allongue, C.H. de Villeneuve, J. Pinson, F. Ozanam, J.N. Chazalviel, X. Wallart, Organic monolayers on Si(111) by electrochemical method, Electrochimica Acta. 43 (1998) 2791–2798. doi:10.1016/S0013-4686(98)00020-6.

[37] C. Mazzara, J. Jupille, W.-Q. Zheng, M. Tanguy, A. Tadjeddine, P. Dumas, Hydrogen-terminated Si(111) and Si(100) by wet chemical treatment: linear and non-linear infrared spectroscopy, Surface Science. 427–428 (1999) 208–213. doi:10.1016/S0039-6028(99)00266-6.

[38] L.-M. Lu, L. Zhang, F.-L. Qu, H.-X. Lu, X.-B. Zhang, Z.-S. Wu, S.-Y. Huan, Q.-A. Wang, G.-L. Shen, R.-Q. Yu, A nano-Ni based ultrasensitive nonenzymatic electrochemical sensor for glucose: Enhancing sensitivity through a nanowire array strategy, Biosensors and Bioelectronics. 25 (2009) 218–223. doi:10.1016/j.bios.2009.06.041.

[39] A. Giacomino, O. Abollino, M. Lazzara, M. Malandrino, E. Mentasti, Determination of As(III) by anodic stripping voltammetry using a lateral gold electrode: Experimental conditions, electron transfer and monitoring of electrode surface, Talanta. 83 (2011) 1428–1435. doi:10.1016/j.talanta.2010.11.033.

[40] A. Giacomino, A. Ruo Redda, S. Squadrone, M. Rizzi, M.C. Abete, C. La Gioia, R. Toniolo, O. Abollino, M. Malandrino, Anodic stripping voltammetry with gold electrodes as an alternative method for the routine determination of mercury in fish. Comparison with spectroscopic approaches, Food Chemistry. 221 (2017) 737–745. doi:10.1016/j.foodchem.2016.11.111.

[41] M. Anderson, C. Ramanan, C. Fontanesi, A. Frick, S. Surana, D. Cheyns, M. Furno, T. Keller, S. Allard, U. Scherf, D. Beljonne, G. D'Avino, E. von Hauff, E. Da Como, Displacement of polarons by vibrational modes in doped conjugated polymers, Phys. Rev. Materials. 1 (2017) 055604. doi:10.1103/PhysRevMaterials.1.055604.

[42] D. Di Nuzzo, C. Fontanesi, R. Jones, S. Allard, I. Dumsch, U. Scherf, E. von Hauff, S. Schumacher, E. Da Como, How intermolecular geometrical disorder affects the molecular doping of donor–acceptor copolymers, Nat Commun. 6 (2015). doi:10.1038/ncomms7460.

[43] Organic Electronics: Emerging Concepts and Technologies, Fabio Cicoira and Clara Santato editors, Wiley-VCH Verlag GmbH & Co. KGaA, Boschstr. 12, 69469 Weinheim, Germany, 2013. http://www.wiley.com/WileyCDA/WileyTitle/productCd-3527411313.html (accessed December 30, 2016).

[44] C. Bruno, F. Paolucci, M. Marcaccio, R. Benassi, C. Fontanesi, A. Mucci, F. Parenti, L. Preti, L. Schenetti, D. Vanossi, Experimental and Theoretical Study of the p- and n-Doped States of Alkylsulfanyl Octithiophenes, J. Phys. Chem. B. 114 (2010) 8585–8592. doi:10.1021/jp9122612.

[45] M. Marcaccio, F. Paolucci, C. Fontanesi, G. Fioravanti, S. Zanarini, Electrochemistry and spectroelectrochemistry of polypyridine ligands: A theoretical approach, Inorganica Chimica Acta. 360 (2007) 1154–1162.

[46] T. Doneux, L. Yahia Cherif, C. Buess-Herman, Controlled Tuning of the Ferri/Ferrocyanide Electron Transfer at Oligo(Ethylene Glycol)-Modified Electrodes, Electrochimica Acta. 219 (2016) 412–417. doi:10.1016/j.electacta.2016.10.005.

[47] Th. Doneux, M. Steichen, A. De Rache, Cl. Buess-Herman, Influence of the crystallographic orientation on the reductive desorption of self-assembled monolayers on gold electrodes, Journal of Electroanalytical Chemistry. 649 (2010) 164–170. doi:10.1016/j.jelechem.2010.02.032.

[48] M. Steichen, Th. Doneux, C. Buess-Herman, On the adsorption of hexaammineruthenium (III) at anionic self-assembled monolayers, Electrochimica Acta. 53 (2008) 6202–6208. doi:10.1016/j.electacta.2008.02.064.

[49] S. Sek, B. Palys, R. Bilewicz, Contribution of Intermolecular Interactions to Electron Transfer through Monolayers of Alkanethiols Containing Amide Groups, J. Phys. Chem. B. 106 (2002) 5907–5914. doi:10.1021/jp013896i.

[50] S. Sek, K. Swiatek, A. Misicka, Electrical Behavior of Molecular Junctions Incorporating α-Helical Peptide, J. Phys. Chem. B. 109 (2005) 23121–23124. doi:10.1021/jp055709c.

[51] R. Michez, J. Vander Steen, T. Doneux, M. Luhmer, C. Buess-Herman, Electroreduction of 1-butyl-3-methylimidazolium bis(trifluoromethanesulfonyl)imide ionic liquid: Oriented product selectivity through the electrode material, Electrochimica Acta. 270 (2018) 434–439. doi:10.1016/j.electacta.2018.03.057.

[52] C. Fontanesi, P. Baraldi, M. Marcaccio, On the dissociation dynamics of the benzyl chloride radical anion. An ab initio dynamic reaction coordinate analysis study, Journal of Molecular Structure: THEOCHEM. 548 (2001) 13–20. doi:10.1016/S0166-1280(00)00863-0.

[53] D. Mishra, T.Z. Markus, R. Naaman, M. Kettner, B. Gohler, H. Zacharias, N. Friedman, M. Sheves, C. Fontanesi, Spin-dependent electron transmission through bacteriorhodopsin embedded in purple membrane, Proceedings of the National Academy of Sciences. 110 (2013) 14872–14876. doi:10.1073/pnas.1311493110.

[54] A. Kumar, E. Capua, K. Vankayala, C. Fontanesi, R. Naaman, Magnetless Device for Conducting Three-Dimensional Spin-Specific Electrochemistry, Angew. Chem. Int. Ed. 56 (2017) 14587–14590. doi:10.1002/anie.201708829.
[55] A. Kumar, E. Capua, C. Fontanesi, R. Carmieli, R. Naaman, Injection of Spin-Polarized Electrons into a AlGaN/GaN Device from an Electrochemical Cell: Evidence for an Extremely Long Spin Lifetime, ACS Nano. 12 (2018) 3892–3897. doi:10.1021/acsnano.8b01347.
[56] C. Fontanesi, Spin-dependent electrochemistry: A novel paradigm, Current Opinion in Electrochemistry. 7 (2018) 36–41. doi:10.1016/j.coelec.2017.09.028.
[57] T. Benincori, S. Arnaboldi, M. Magni, S. Grecchi, R. Cirilli, C. Fontanesi, P. Romana Mussini, Highlighting spin selectivity properties of chiral electrode surfaces from redox potential modulation of an achiral probe under an applied magnetic field, Chemical Science. (2019). doi:10.1039/C8SC04126A.
[58] K. Ray, S.P. Ananthavel, D.H. Waldeck, R. Naaman, Asymmetric Scattering of Polarized Electrons by Organized Organic Films of Chiral Molecules, Science. 283 (1999) 814–816. doi:10.1126/science.283.5403.814.
[59] P.C. Mondal, C. Fontanesi, D.H. Waldeck, R. Naaman, Spin-Dependent Transport through Chiral Molecules Studied by Spin-Dependent Electrochemistry, Acc. Chem. Res. (2016). doi:10.1021/acs.accounts.6b00446.
[60] R. Landauer, Spatial Variation of Currents and Fields Due to Localized Scatterers in Metallic Conduction, IBM Journal of Research and Development. 1 (1957) 223–231. doi:10.1147/rd.13.0223.
[61] C. Cuevas, E. Scheer, Molecular Electronics | World Scientific Series in Nanoscience and Nanotechnology, World Scientific Publishing Co. Pte. Ltd., Singapore, 2017. https://www.worldscientific.com/worldscibooks/10.1142/7434.
[62] K. Michaeli, D.N. Beratan, D.H. Waldeck, R. Naaman, Voltage-induced long-range coherent electron transfer through organic molecules, PNAS. 116 (2019) 5931–5936. doi:10.1073/pnas.1816956116.
[63] T. Lee, W. Wang, M.A. Reed, Mechanism of Electron Conduction in Self-Assembled Alkanethiol Monolayer Devices, Annals of the New York Academy of Sciences. 1006 (2003) 21–35. doi:10.1196/annals.1292.001.
[64] J.J. Kushmerick, S.K. Pollack, J.C. Yang, J. Naciri, D.B. Holt, M.A. Ratner, R. Shashidhar, Understanding Charge Transport in Molecular Electronics, Annals of the New York Academy of Sciences. 1006 (2003) 277–290. doi:10.1196/annals.1292.019.
[65] R. Gutierrez, E. Díaz, C. Gaul, T. Brumme, F. Domínguez-Adame, G. Cuniberti, Modeling Spin Transport in Helical Fields: Derivation of an Effective Low-Dimensional Hamiltonian, J. Phys. Chem. C. 117 (2013) 22276–22284. doi:10.1021/jp401705x.
[66] A.C. Aragonès, E. Medina, M. Ferrer-Huerta, N. Gimeno, M. Teixidó, J.L. Palma, N. Tao, J.M. Ugalde, E. Giralt, I. Díez-Pérez, V. Mujica, Measuring the Spin-Polarization Power of a Single Chiral Molecule, Small. 13 (2017) 1602519. doi:10.1002/smll.201602519.
[67] K. Michaeli, R. Naaman, Origin of Spin-Dependent Tunneling Through Chiral Molecules, J. Phys. Chem. C. 123 (2019) 17043–17048. doi:10.1021/acs.jpcc.9b05020.
[68] J.-T. Li, Z.-Y. Zhou, I. Broadwell, S.-G. Sun, In-Situ Infrared Spectroscopic Studies of Electrochemical Energy Conversion and Storage, Acc. Chem. Res. 45 (2012) 485–494. doi:10.1021/ar200215t.
[69] J.A. Pople, Gaussian suite of programs, Wallingford, Connecticut, 2017. http://gaussian.com/ (accessed April 18, 2017).
[70] P.C. Mondal, N. Kantor-Uriel, S.P. Mathew, F. Tassinari, C. Fontanesi, R. Naaman, Chiral Conductive Polymers as Spin Filters, Adv. Mater. 27 (2015) 1924–1927. doi:10.1002/adma.201405249.
[71] P.C. Mondal, C. Fontanesi, D.H. Waldeck, R. Naaman, Field and Chirality Effects on Electrochemical Charge Transfer Rates: Spin Dependent Electrochemistry, ACS Nano. 9 (2015) 3377–3384. doi:10.1021/acsnano.5b00832.

[72] A.J. Bard, L.R. Faulkner, Wiley: Electrochemical Methods: Fundamentals and Applications, 2nd Edition, Wiley, New York, 2001. http://eu.wiley.com/WileyCDA/WileyTitle/productCd-0471043729.html.
[73] A.S. Bondarenko, G.A. Ragoisha, Inverse Problem In Potentiodynamic Electrochemical Impedance (pp. 89-102), n.d. http://www.novapublishers.org/catalog/product_info.php?products_id=2337 (accessed May 7, 2019).
[74] G. Perluzzo, G. Bader, L.G. Caron, L. Sanche, Direct determination of electron band energies by transmission interference in thin films, Physical Review Letters. 55 (1985) 545–548.
[75] L.G. Caron, G. Perluzzo, G. Bader, L. Sanche, Electron transmission in the energy gap of thin films of argon, nitrogen, and n-hexane, Physical Review B. 33 (1986) 3027.
[76] S. Sek, A. Misicka, R. Bilewicz, Effect of Interchain Hydrogen Bonding on Electron Transfer through Alkanethiol Monolayers Containing Amide Bonds, J. Phys. Chem. B. 104 (2000) 5399–5402. doi:10.1021/jp000376z.
[77] P.C. Mondal, W. Mtangi, C. Fontanesi, Chiro-Spintronics: Spin-Dependent Electrochemistry and Water Splitting Using Chiral Molecular Films, Small Methods. 2 (2018) 1700313. doi:10.1002/smtd.201700313.
[78] C. Fontanesi, E. Capua, Y. Paltiel, D.H. Waldeck, R. Naaman, Spin-Dependent Processes Measured without a Permanent Magnet, Advanced Materials. 30 (2018) 1707390. doi:10.1002/adma.201707390.